Nonlinear Soil Response in the Near-Field of a Vibrator Truck: Application to Land Seismic Surveys

Fred Pearce, Mark Willis, Dan Burns, and M. Nafi Toksöz
Earth Resources Laboratory
Dept. of Earth, Atmospheric, and Planetary Sciences
Massachusetts Institute of Technology
Cambridge, MA 02139

Paul Johnson
Geophysics Group
Los Alamos National Laboratory
Los Alamos, NM 87545

Abstract

The nonlinear behavior of soils can significantly modify the wavelet radiated from vibrator trucks. In this paper, we describe a field experiment designed to measure the nonlinear response of a natural soil formation in the near-field of a vibrator truck. A 267-kN (30-ton) vibrator truck performed a step-sweep through a set of 201 discrete frequencies from 50-Hz to 10-Hz, which was repeated at 11 increasing source amplitudes. Steady-state amplitude spectra for the source output measured on the vibrator truck are significantly different than amplitude spectra for receivers located immediately adjacent to the vibrator truck. Spectral ratios between the source and adjacent receivers show a systematic decrease in peak frequency as the source amplitude is increased. Near-field measurements from vibrator trucks provide a more accurate measurement of the source wavelet that includes soil nonlinearity, and may ultimately lead to a method for optimizing the transmission of energy through an arbitrary soil formation.

1 Introduction

The complex nature of near-surface soils poses a major challenge to acquiring high-quality seismic data on land. Vibrator trucks are the most common sources employed during land-based data acquisition and have been well studied by many researchers (Miller, 1954; Sallas, 1984; Lebedev, 2006). Many seismic processing techniques require estimates of the source wavelet for correlating with recorded waveforms. The output wavelet from the source is typically estimated using instruments on the vibrator truck to calculate the ground force delivered to the ground. However, Sallas (1984) showed that borehole ground motions directly beneath a vibrator truck vary depending

on the source amplitude and the soil type beneath the source plate.

The variability of borehole ground motion with source amplitude is consistent with laboratory experiments on the nonlinear behavior of soils which show a decrease in soil modulus and Q as dynamic strain amplitude increases above approximately 10^{-6} (Hardin, 1972; Seed, 1986). These strain values are easily realized in the near-field of a vibrator truck. The magnitude of the nonlinear soil response is largest when confining pressures are lowest, and different soil types may have very different nonlinear properties (Seed, 1986). We expect strong nonlinear soil behavior in the near-field of a vibrator truck, which may vary from shot point to shot point. Furthermore, the presence of shallow impedance contrasts may further complicate the transmission of energy through the soils by trapping energy near the source. Therefore, we expect near-surface soils to strongly alter the radiated wavelet from a vibrator truck in ways that may not be observed from measurements on the vibrator truck alone.

In this paper we describe a pilot field experiment to measure the nonlinear response of a natural soil formation in the near-field of a vibratory truck. The Methods section, describes the field site location, instrumentation and experiment protocol. The Data section shows the experiment data and discusses important source characteristics for subsequent analysis. The Analysis & Results section describes each step of the analysis procedure used to calculate steady-state spectral ratios from our experiment data. The purpose of this work is to document the nonlinear nature of ground motion in the near-field of a vibrator truck with the ultimate goal of obtaining accurate measurements of the wavelet transmitted through the soil formation.

2 Methods

2.1 Site description

The experiment site is located at the Capitol Aggregates Test Site near Austin, Texas where 11-m of young, unconsolidated point bar sediments overlie a soft shale. The site was selected primarily because of extensive site characterization work previously conducted by Kurtulus et al. (2005). Near-surface soils consist of predominately non-plastic silt (ML) with intermittent silty sand (SM) based on borehole soil samples. Results from the Spectral Analysis of Surface Waves (SASW) method provided a shear velocity profile (Kurtulus et al., 2005), which we supplemented with a shallow refraction survey to constrain near surface P-wave velocity (Figure 1). The resulting velocity profile shows a general increase in wave-speeds with increasing depth and significant impedance contrasts at depths of 2-m, 4.5-m, 7-m (water table) and 11-m (shale). Although not shown, laboratory tests were also conducted on borehole samples to obtain modulus and damping degradation curves for quantitative comparison with future work.

2.2 Instrumentation

The source used is a large vibrator truck with a maximum vertical force output of approximately 267 kN (60,000 lbf). The source couples to the ground via a 2x2 m plate and is capable of shaking over a broad frequency band (~10-180 Hz). A function generator controls the frequency and amplitude of the source, while accelerometers built into the truck estimate the resulting force output to the ground. The input function generator signals and the corresponding force output are recorded for analysis.

In this study, we only consider vertical motion of the source recorded at four receivers with increasing distance from the source as shown in Figure 1. The receivers used are Kinemetrics three-component accelerometers designed for large accelerations (> 2g). Our array extends along a N-S line

from the source. Each receiver is anchored to a concrete pad with diameter of approximately 0.35 m (much smaller than expected wavelengths). The concrete pads were designed to match the soil density and each pad was approximately the same dimensions. All recorded time signals (source and receivers) have a time sampling of 0.005 sec and are converted to SI units of acceleration (m/s/s) using appropriate instrument corrections.

2.3 Source protocol

We measure the soil response at discrete frequencies within a limited band following the methodology employed in Nonlinear Resonance Ultrasound Spectroscopy (NRUS) (Guyer and Johnson, 1999). The source protocol is a down-sweep through M=201 discrete frequencies beginning at 50-Hz (f_1) and decreasing with frequency step-size of 0.2-Hz (df) as follows:

$$f_m = f_1 - (m-1)\, df, \quad m = 1, \ldots, M. \qquad (1)$$

The down-sweep decreases in frequency as a function of time to a minimum frequency of 10-Hz. The source was held at each frequency for 40 cycles to be certain steady-state conditions were reached. We repeat the down-sweep described in equation 1 at N=11 source amplitudes beginning at an input voltage of 0.2-V (A_1) with a step-size of 0.2-V (dA) as follows:

$$\mathrm{A}_n = \mathrm{A}_1 + (n-1)\, d\mathrm{A}, \quad n = 1, \ldots, N. \qquad (2)$$

We present equation 2 in terms of input voltage because it is the independent parameter that we control via the function generator signal. Based on this source protocol, we obtain acceleration time series for the source and receivers, which contain the steady-state system response at each frequency f_m and each source amplitude A_n.

3 Data

We present the data from our experiment and describe important data characteristics that will help guide subsequent analysis. Figure 2 shows a comparison between the input voltage from the function generator to the source (converted to equivalent acceleration) and the measured source-ground acceleration output from the vibrator truck for the entire experiment duration. While both down-sweeps and up-sweeps (frequencies step from high to low and then low to high, respectively) are shown for completeness, only down-sweeps are discussed in this paper. The vibrator truck produces variable amplitudes across the step-sweep band and is especially unstable at low frequency (<15 Hz). At low source amplitudes, the measured source amplitude decreases as the source frequency decreases, while at high source amplitudes the measured source amplitude shows some variation across a step-sweep but is relatively constant. The measured source output clipped at 2g for the two largest source amplitudes, an observation consistent with the dynamic range set for the instruments, thereby verifying the data were correctly converted from counts to m/s/s.

We observe a clear difference between the receiver acceleration time signals (Figure 3) and the measured source-ground acceleration time signals from the source (Figure 2). As expected, the receiver signals have smaller peak amplitudes than those for the measured source output. The differences in amplitudes between the source and receivers are due to strong dissipation most likely attributable to near-source effects. Both components have more pronounced spikes in amplitude as compared to the measured source acceleration, particularly the N-S component. For the vertical

component, there is a slight decrease in amplitude with distance from the source; however, the N-S component has the largest acceleration amplitudes at receivers R2 and R3.

We have shown that the receiver signals are significantly more complex than the measured source output. However, vibrator trucks are well known to generate significant harmonic amplitudes, particularly at their low-frequency limit where coupling becomes inefficient (Solodov & Beresnev, 2006). Based on the time signals, we have no way of distinguishing whether most of the amplitude we observe is at the fundamental frequency or associated with harmonics. To gain insight into the relative contribution of harmonics, we consider the analytic signal representation of our experimental data. The analytic representation refers to a complex signal (X_A) in which the real part is the original experimental data (X_D) and the imaginary part is the 90˚ phase shifted version of the original data obtained from the Hilbert transform (X_H)

$$X_A(t) = X_D(t) + iX_H(t). \qquad (3)$$

The magnitude of the analytic signal is defined as the envelope (E),

$$E(t) = \sqrt{\left[X_D(t)^2 + X_H(t)^2\right]}, \qquad (4)$$

and the phase angle of the analytic signal is defined as the instantaneous phase (ϕ)

$$\phi(t) = \tan^{-1}\left(\frac{X_H(t)}{X_D(t)}\right) \qquad (5)$$

where $\tan^{-1}$ is the four quadrant inverse tangent function. In the case of step-sweeps, it is more instructive to consider the instantaneous frequency (Ω) obtained from the 1st time derivate of the unwrapped, instantaneous phase

$$\Omega(t) = \frac{d\phi^u(t)}{2\pi dt} \qquad (6)$$

where the superscript *u* denotes the unwrapped phase and 2π converts radians to Hz.

Figure 4a shows the instantaneous frequency and amplitude envelope for unfiltered down-sweeps from the function generator and the measured source output. We now see the advantage of the analytic representation for a discrete step-sweep. The instantaneous frequency and amplitude give the exact frequency and amplitude of a monotone time signal, as illustrated by the function generator input (red curves in Figure 4a). However, when harmonics are present, the instantaneous frequency and amplitude envelope are more complicated but tend to center about the frequency and amplitude of the dominant component (i.e. the component with largest amplitude). Any smaller amplitude components will generate scatter in the instantaneous frequency and amplitude envelope about the amplitude and frequency of the dominant component. Therefore, the instantaneous frequency for the measured source output (black curves, top plot of Figure 4a) suggests that the source is following the time-frequency protocol we specified, as it is centered on the input function generator instantaneous frequency. Note that at 50-Hz all harmonics will be removed by an anti-aliasing filter with cut-off frequency of approximately 90-Hz. The scatter in the instantaneous frequency and amplitude envelopes of the measured source output gives a relative measure of the harmonic distortion generated

by the source.

Filtering the time signals to include only frequency components within the down-sweep band only slightly reduces the observed scatter (Figure 4b). The instantaneous frequency may reach outside the filter band if the dominant frequency component in the signal (which controls the mean value of the instantaneous frequency) is near the edge of the filter band, and other frequencies are present within the pass band (which controls the amount of scatter). The general increase in scatter with decreasing source frequency is due to increasing amplitudes of the harmonics relative to the fundamental and harmonics of increasing order falling within the pass-band of the filter. The latter case can be thought of as follows: a fundamental frequency of 50-Hz has no harmonics in the pass-band while at 10-Hz we have 4 harmonics (20-Hz, 30-Hz, 40-Hz, and 50-Hz) in the pass-band (10-Hz to 50-Hz). The instantaneous frequency and amplitude envelopes show less scatter at large source amplitudes, which suggests that harmonic distortion is most severe at low source amplitudes.

The overlap between harmonics and fundamental frequencies must be addressed when designing an analysis method to extract the amplitude of each fundamental frequency in the step-sweep. We cannot simply Fourier transform the entire time signals and preserve the fundamental amplitudes because the amplitudes at high frequencies will be contaminated with the harmonics at low frequencies, regardless of filtering. Therefore, we turn to a time-frequency analysis to process our data as described in the following section.

4 Analysis and Results

In this section, we describe the analysis procedure and present the results obtained from our experiment data. We first describe the time-frequency analysis used to extract the steady-state amplitude at each frequency in the step-sweep. Based on this analysis, we construct steady-state amplitude spectra for every time signal recorded during our experiment. Finally, we use spectral ratios to characterize the nonlinear soil response from the amplitude spectra.

4.1 Time-frequency analysis

We use a homodyne for our time-frequency analysis, which we will describe as it applies to a single acceleration time signal recording a down-sweep. The time signal is dissected into a series of time windows, $\ddot{u}_w$, where the subscript *w* refers to the window location in the time signal. Each window has a constant number of time samples, *T*, and in general the windows may overlap. We construct two ortho-normal, monochromatic time signals with frequency f_m, an in-phase component I_m and quadrature component Q_m. The RMS acceleration amplitude is then computed for each frequency and each time window

$$R_{w,m} = \sqrt{\left(\frac{2}{T}\right)\left[\left(I_m \bullet \ddot{u}_w\right)^2 + \left(Q_m \bullet \ddot{u}_w\right)^2\right]} \quad (7)$$

where $\bullet$ denotes the vector dot product. In practice, the number of time samples in the analysis window may be adjusted based on the frequency, f_m, and a cosine taper is applied to each $\ddot{u}_w$ to smooth the edges. The output from the time-frequency analysis is a 2D matrix of RMS amplitudes with each row referring to a single frequency in the step-sweep and each column referring to the temporal location of the analysis window.

Figure 5 shows an example output from the time-frequency analysis for the measured source

response and the vertical component of acceleration at R3. The method is able to clearly separate the harmonics from the fundamental frequencies and is consistent with the input time-frequency protocol. For the measured source output, the amplitude at the fundamental frequency is dominant across the entire down-sweep. For the receiver, the amplitude at the fundamental is only dominant down to approximately 20-Hz and then falls off rapidly, at which point the harmonic amplitudes are similar to the fundamental amplitude.

4.2 Amplitude spectra

We compute steady-state amplitude spectra for every time signal by extracting the RMS amplitude at steady-state for each discrete frequency in the down-sweep. Figure 6 shows the steady-state amplitude spectra from the function generator input and the measured source output for all source amplitudes. The amplitude spectra for the function generator input are constant across the frequency band, while the amplitude spectra for the measured source output peak near 50-Hz and generally decrease in amplitude as the source frequency decreases. For large source amplitudes, the amplitude spectra have significant structure from 50-Hz down to about 18-Hz and then fall off rapidly.

The steady-state amplitude spectra for the receiver components are significantly more complicated than the measured source spectra (Figure 7). At the lowest source amplitude, the receiver spectra are all similar in structure, as opposed to larger source amplitudes where the character of the spectra are more complex and vary depending on receiver location and component. Distinct peaks are observed in the receiver amplitude spectra, particularly for the vertical component, and these peaks appear to shift slightly as the source amplitude increases. In general, the receiver spectra tend to have broad peaks that make it difficult to observe changes in the spectra with increasing source amplitude.

4.3 Spectral ratios

We compute spectral ratios using the source spectra to normalize each receiver spectra. This approach is typically applied in the laboratory to derive the resonance modes of a sample with finite-dimensions (Guyer & Johnson, 1999). Formally, we calculate the spectral ratio, $G(x_i;x_0)$, by dividing the receiver spectra recorded at x_i by the source spectra recorded at x_0 such that

$$G_{n,m}(x_i;x_0) = \frac{R_{n,m}(x_i)}{S_{n,m}(x_0)} \qquad (8).$$

$G(x_i;x_0)$ is a 2D matrix with each row corresponding to a source amplitude (A_n), each column corresponding to a fundamental frequency of the down-sweep (f_m), and the matrix values corresponding to the spectral ratio amplitudes.

Figure 8 shows $G(x_i;x_0)$ obtained for the vertical component and N-S components. As the source amplitude increases, we observe a smooth change in the structure of the spectral ratios. In general, peaks in the spectral ratios decrease to lower frequencies as the source amplitude is increased. This trend is remarkably similar for all receiver components. The peaks with the largest amplitudes (between 40-Hz to 50-Hz at the lowest source amplitude) decrease in frequency by as much as 35%. The spectral ratios all show a strong fall-off in amplitude at an apparent cut-off frequency. The spectral ratios tend to have broad peaks that vary between 0.15 and 0.25. However, the behavior of the peaks and the location of the apparent cut-off frequency strongly depend on receiver location and component. For vertical components, the spectral ratios nearest the source ($G(x_1;x_0)$) maintain a relatively constant amplitude as the source amplitude increases. Conversely, the spectral ratios

furthest from the source tend to decrease in amplitude most rapidly with increasing source amplitude. The apparent cut-off frequency for the vertical components decreases with source amplitude from about 25-Hz at the lowest source amplitude to about 20-Hz at the highest source amplitude. For the N-S components, we observe the opposite behavior with the spectral ratio amplitudes nearest the source increasing with increasing source amplitude, while the spectral ratio amplitudes furthest from the source remain relatively constant with increasing source amplitude. A clear cut-off frequency is not observed for the N-S component nearest the source but develops clearly at the furthest receiver where it varies from 30-Hz to 20-Hz.

The similarities between the spectral ratios for different receivers and the large amount of dissipation point to a potential dominance of the source-ground contact region. The contact region is known to produce large harmonic distortion (Lebedev et al., 2006), which may be responsible for the large apparent dissipation.

5 Conclusions

In this study, we developed a novel approach for measuring the nonlinear response of a natural soil formation in the near-field of a vibrator truck. Steady-state amplitude spectra for receivers adjacent to the vibrator truck are remarkably different than the ground force measured on the vibrator truck. Spectral ratios between the receiver components and the source show a rapid decrease in peak frequency as the source amplitude is increased, which is clear evidence of nonlinear soil behavior. Our work suggests that measurements obtained in the near-field of vibrator trucks may capture the effects of nonlinear soil behavior on the radiated wavelet from vibrator trucks. Therefore, such measurements may lead to significant improvements in seismic images from land-based surveys by providing a more accurate source wavelet. Furthermore, near-field measurements may provide a means to optimize the transmission of energy through the soil column by adaptively varying the source amplitude at different frequencies to minimize the energy trapped in the near-surface. Further studies will be required to understand the relationship between surface observations and the wavelet transmitted through the soil to depth, and to generalize our field procedure to smoothly varying frequency modulated signals such as Chirps.

6 Acknowledgements

This work is funded by the ERL Founding Members Consortium. Additional support comes from the Institute of Geophysics and Planetary Physics at Los Alamos National Laboratory.

References

Guyer, R. A., and P. A. Johnson (1999), The astonishing case of mesoscopic elastic nonlinearity, *Physics Today*, *52*, 30-35.

Hardin, B. O. (1972), Shear modulus and damping in soils: design equations and curves, *Journal of Soil Mechanics and Foundation Division, 98*, 667-692.

Johnson, P. A., B. Zinszner, P. N. J. Rasolofosaon, F. Cohen-Tenoudji, and K. E. A. Van Den Abelle (2004), Dynamic measurements of the nonlinear elastic parameter alpha in rock under varying conditions, *J. Geophys. Res.-Solid Earth*, *109*, 2202.

Kurtulus, A., J. J. Lee, and K. H. Stokoe (2005), Summary report: site characterization of Capital Aggregates test site, *University of Texas, Austin Internal Report*, 1-47.

Lamb, H. (1904), On the propagation of tremors over the surface of an elastic solid, *Philosophical Transactions of the Royal Society, A203*, 1.

Lebedev, A. V., I. A. Beresnev, P. L. Vermeer (2006), Model parameters of the nonlinear stiffness of the vibrator-ground contact determined by inversion of vibrator accelerometer data, *Geophysics*, 7, H25-H32.

Miller. G. F., and H. Pursey, 1954, The field and radiation pattern of mechanical radiators on the free surface of a semi-infinite isotropic solid, *Proc. Royal. Society, 223*, p, 521-541.

Muravskii, G. (2005), On description of hysteretic behaviour of materials, *International Journal of Solids and Structures, 42*, 2625-2644.

Sallas, J. J. (1984), Seismic vibrator control and the downgoing P-wave, *Geophysics, 49*, 732-740.

Seed, H. B. (1986), Moduli and damping factors for dynamic analyses of cohesionless soils, *Journal of Geotechnical Engineering, 112*, 1016-1032.

Van Den Abeele, K. E. A., J. Carmeliet, P. A. Johnson, and B. Zinszner (2002), Influence of water saturation on the nonlinear elastic mesoscopic response in Earth materials and the implications to the mechanisms of nonlinearity, J. Geophys. Res.-Solid Earth, 107, 2121.

Xu, Y., J. Xia, and R. D. Miller (2006), Quantitative Estimation of Minimum Offset for Multichannel Surface-Wave Survey with Actively Exciting Source, J. Applied Geophys., 59, 117-125.

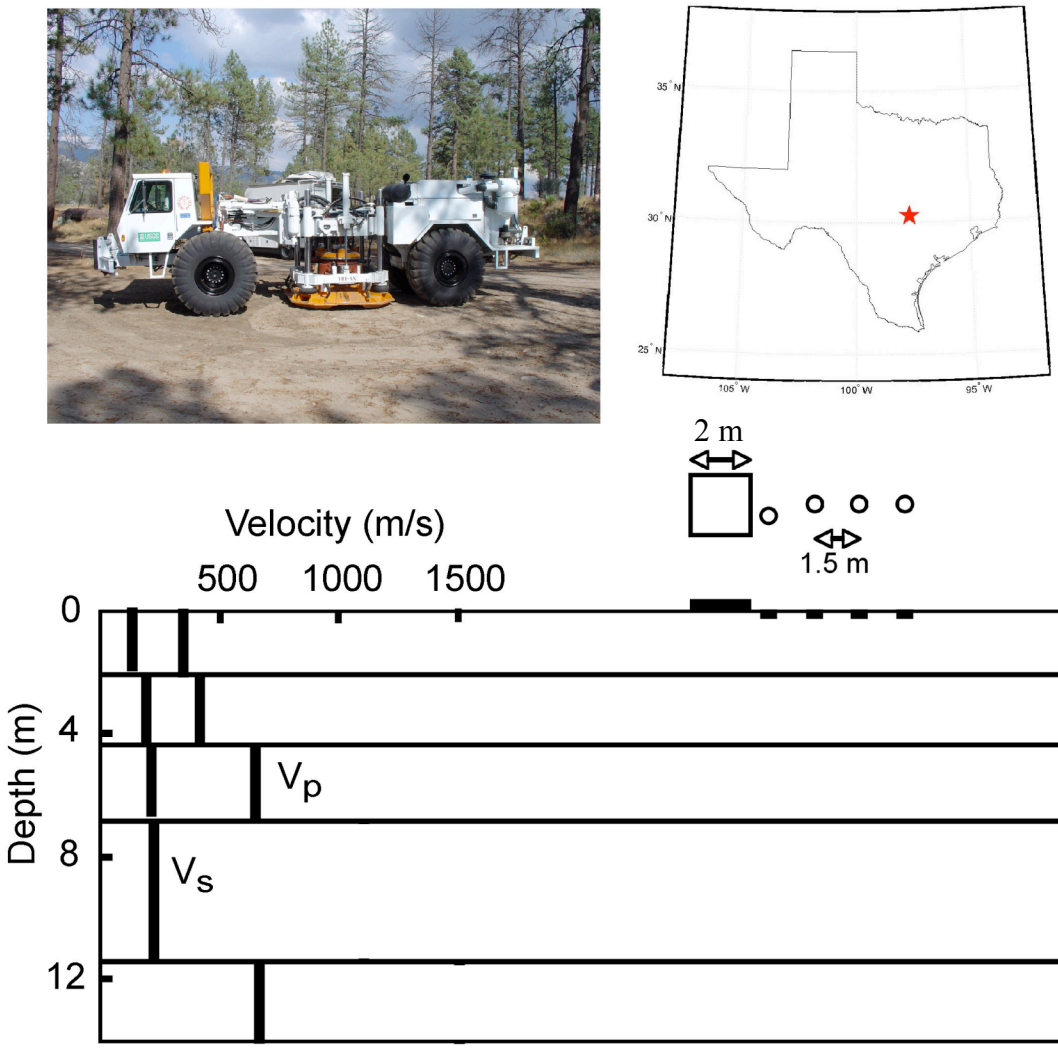

Figure 1: Field site description: Velocity profile and instrument layout.

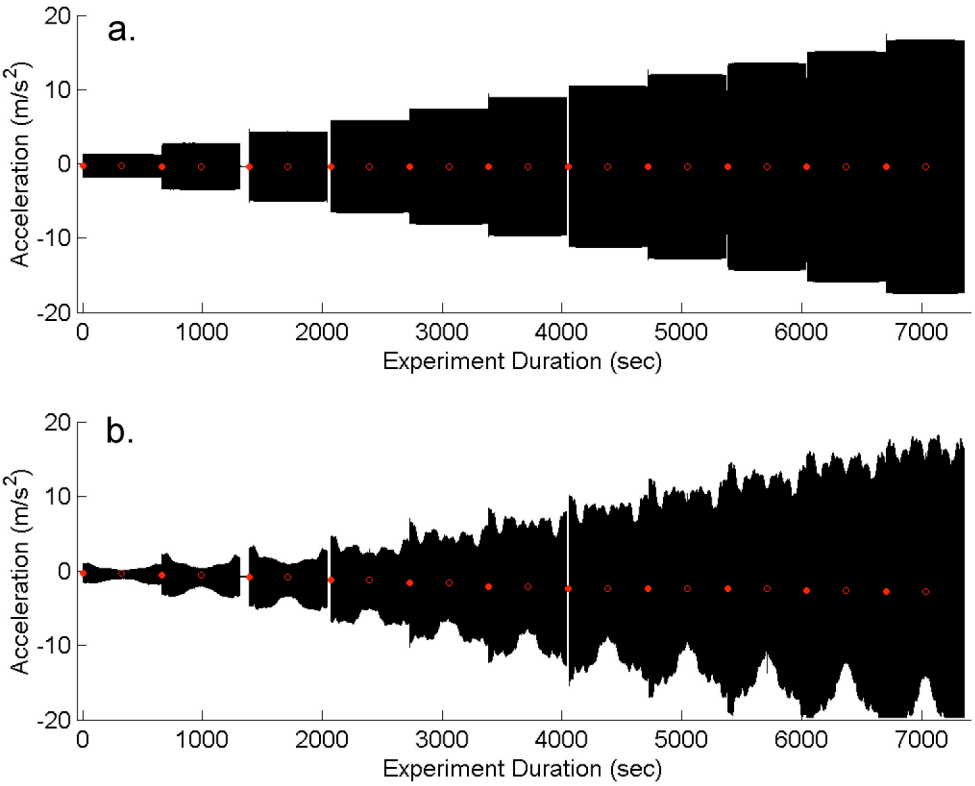

Figure 2: Unfiltered time signals for entire experiment from a) source input and b) measured source-ground contact. Filled circles denote down-sweep start times (amplitude changes), and open circles mark switches from down-sweeps to up-sweeps (amplitude constant). Time duration of each step-sweep is approximately 325 s.

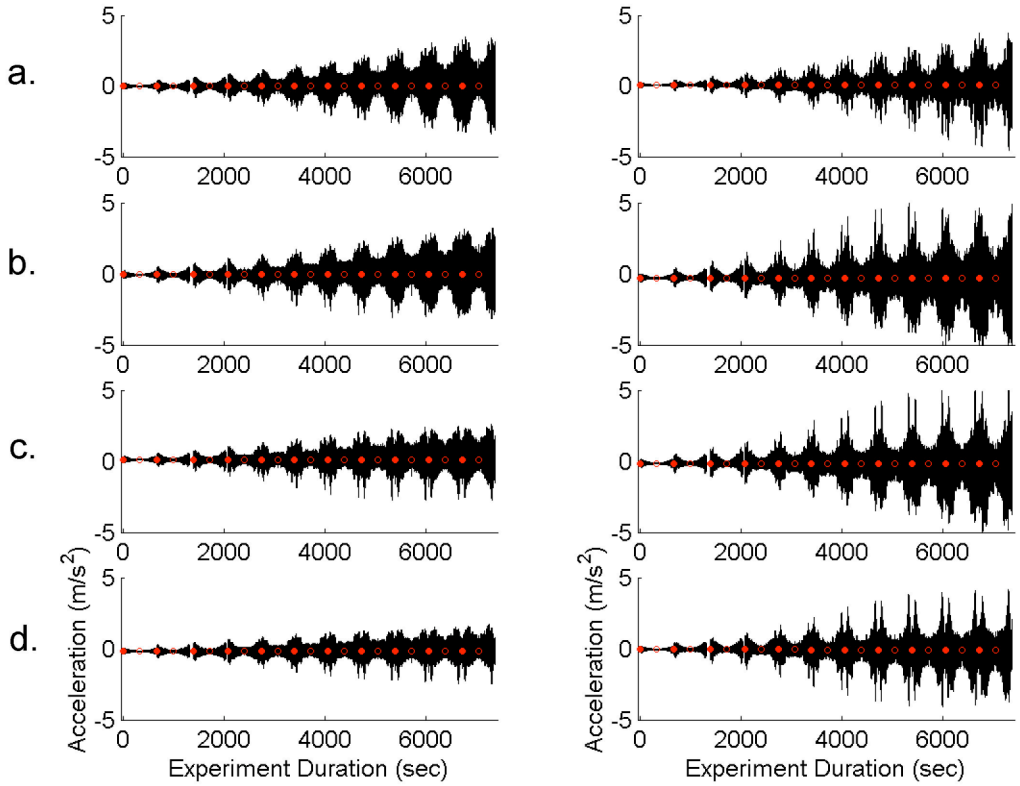

Figure 3: Unfiltered time signals for vertical component (left) and N-S component (right) recorded at R1-R4 corresponding to (a-d), respectively. Notation same as Figure 2.

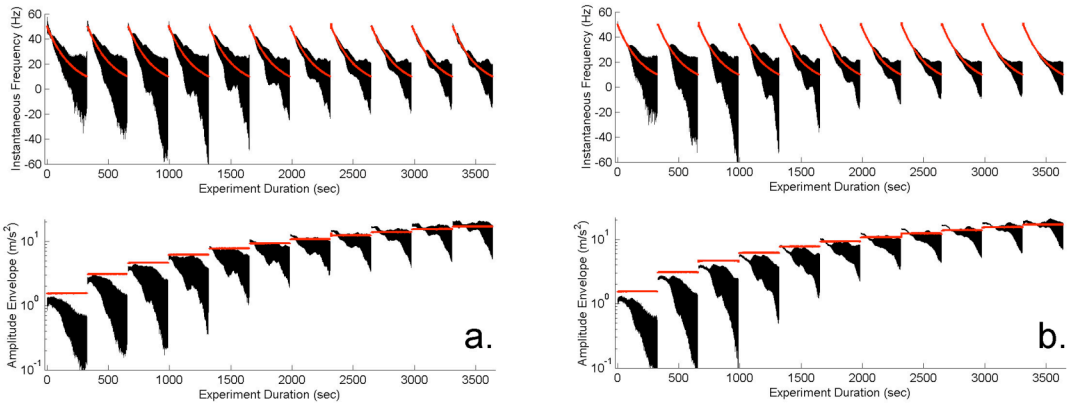

Figure 4: Instantaneous frequency and amplitude envelope of unfiltered time signals from input function generator (red) and measured source-ground contact (black): a) unfiltered and b) band-pass filtered from 10-Hz to 50-Hz. Note that the function generator results in b) have also been filtered to verify filter response.

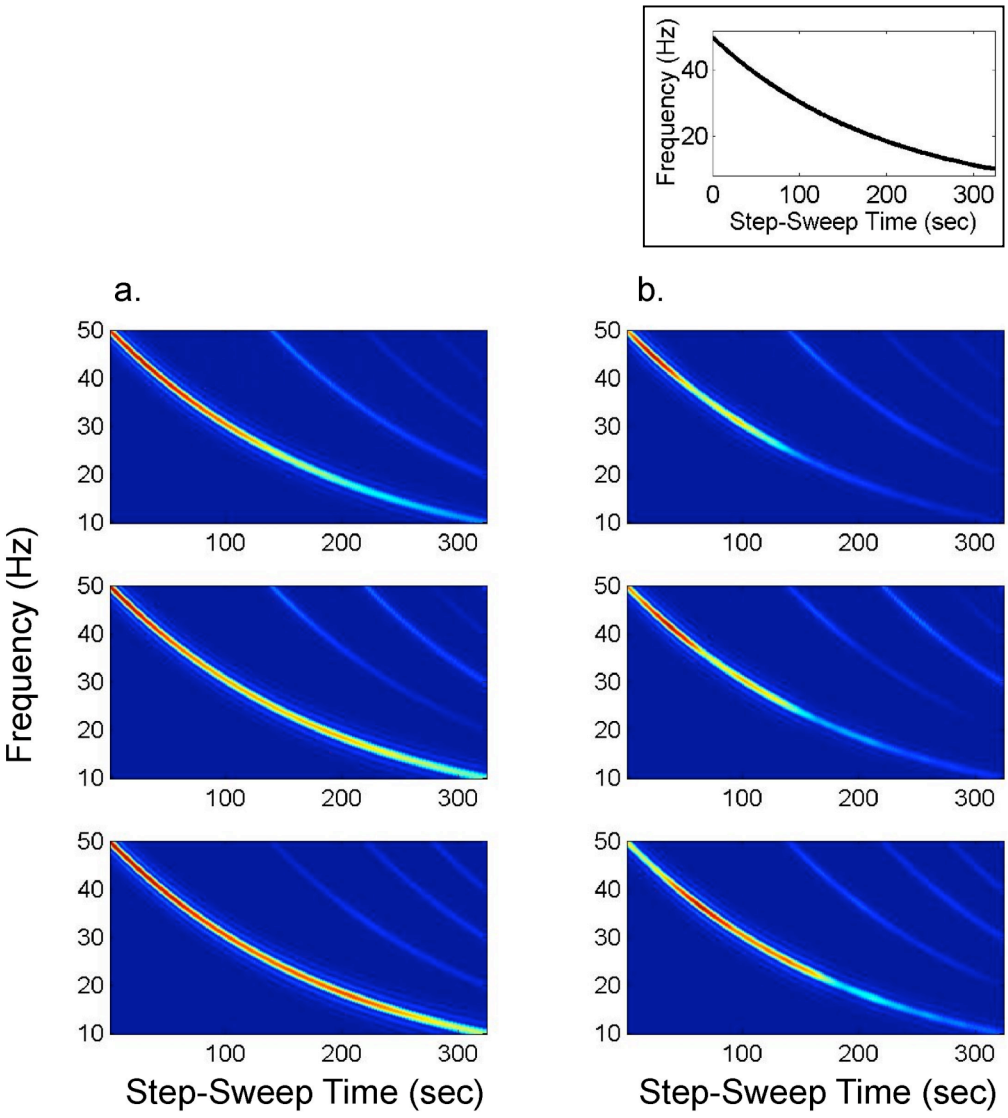

Figure 5: Results of time-frequency analysis at source amplitudes A1 (top), A5 (middle), and A10 (bottom): a) the measured source output and b) the vertical component of R3. Note the similarity between the input time-frequency protocol (inset) and the peak amplitudes of each panel.

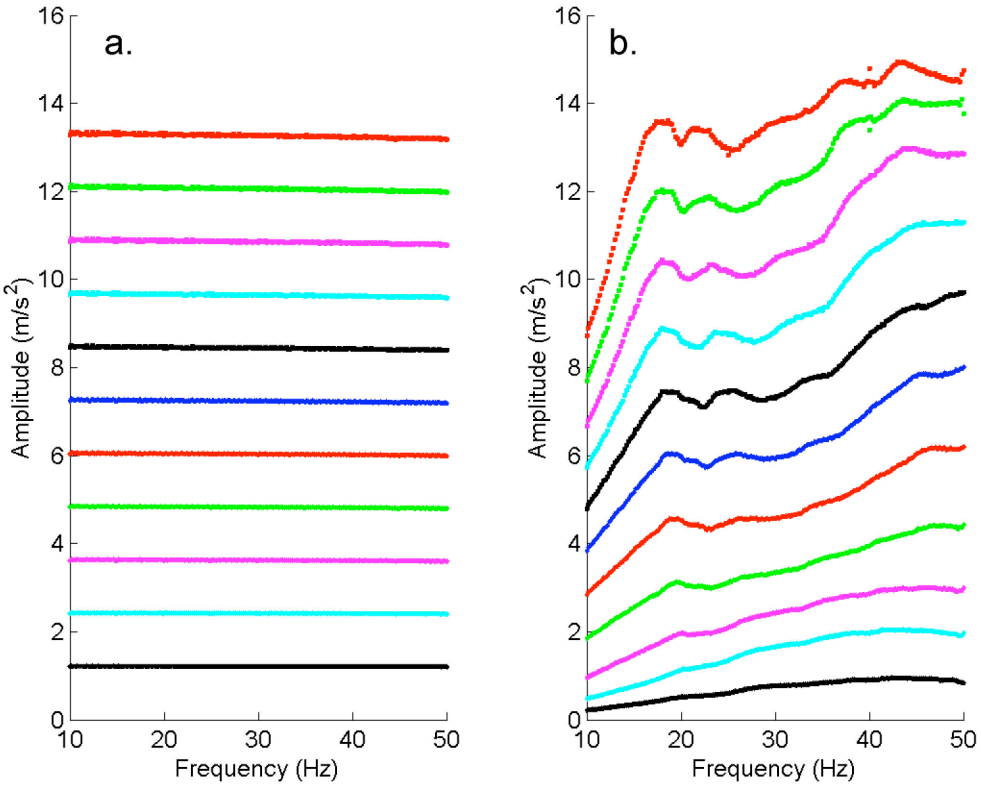

Figure 6: Steady-state amplitude spectra for a) the function generator input and measured source output.

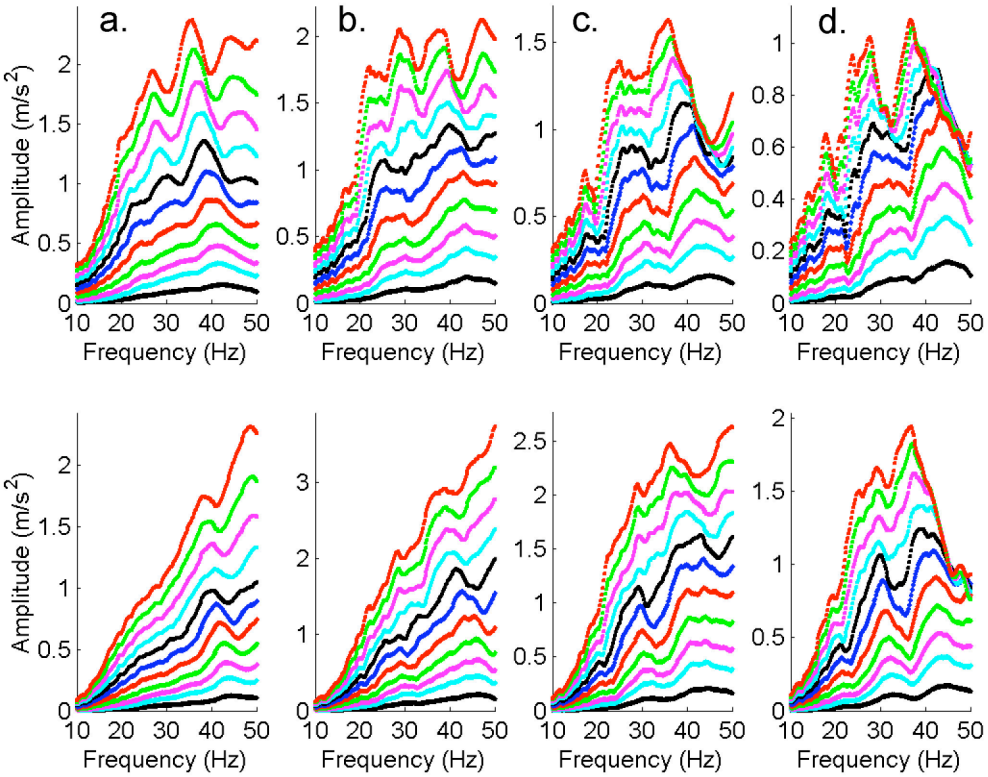

Figure 7: Steady-state amplitude spectra for vertical components (top) and N-S components (bottom) of receivers a)R1, b) R2, c) R3, and d) R4.

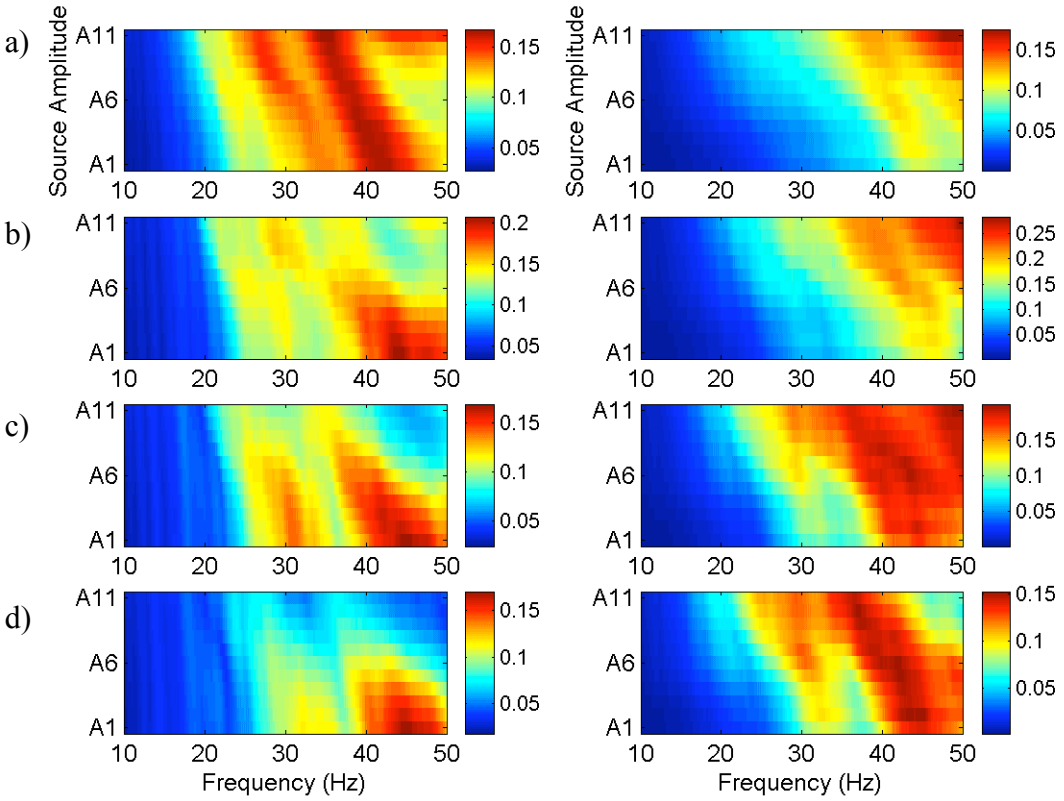

Figure 8: Spectral ratios referenced to the measured source output for vertical components (left) and N-S components (right): a) R1, b) R2, c) R3, d) R4.